Nonlinear Analysis of Ferrocement Flexural Beams

Dr. Ihsan A.S. Al-Shaarbaf
Engineering College, University of Al-Nahrain/Baghdad
Dr. Nisreen S. Mohammed
Building and Construction Engineering Department, University of Technology/Baghdad
E-mail: nisreen_alnimer@yahoo.com

Received on: 18/3/2012 & Accepted on: 15/8/2012

ABSTRUCT

This paper aims to study the behavior and strength of ferrocement beams under flexural loading. Seven specimens (four simply supported rectangular beams and three simply supported T-beams) are tested under flexural load. An analytical method is proposed to analyze the ferrocement beams. A three-dimensional finite element computer program is developed in this paper to study the nonlinear behavior of ferrocement beams. The quadratic 20-node brick elements are used to model the mortar. The wire mesh layers are considered as smeared layers embedded within the brick element. The skeletal bars are modeled as axial members embedded within the brick element. Material nonlinearity due to the response of mortar in compression, crushing, cracking in tension, tension stiffening and shear retention effect of cracked mortar and yielding of wire mesh and skeletal bar are considered. Good agreement between the experimental work results, the analytical and the finite element results are achieved.

Keywords: cross section, type of wire mesh, layered of wire mesh, skeletal reinforcement.

التحليل اللاخطي وسعة تحمل الانحناء للعتبات الفيروسمنتية

الخلاصه

يتضمن هذا دراسه سلوك ومدى سعه التحمل للعتبات المصنوعه من الفيروسمنت تحت تأثير الانحناء. تم صب سبع نماذج (اربعه منهاعتبات بسيطة الاسناد ذات مقطع مستطيل وثلاثه عتبات مجنحة بسيطة الاسناد ذات مفطع على شكل حرف T)، وتم فحصها تحت تأثير الانحناء. وتم اعتماد التحليل النظري، تطوير برنامج حاسوبي يعتمد على طريقة العناصر المحددة كوسيلة لدراسة تصرف الاعضاء السمنت المعدنية. استخدمت العناصر ثلاثية الابعاد ذات العشرين عقدة لنمذجة المونة. تم تمثيل المشبكات الحديدية كطبقة حديدية بسمك مكافئ منتشرة داخل العنصر الطابوقي كما تم تمثيل حديد التسليح الهيكلي على شكل عناصر محورية مطمورة داخل العنصر الطابوقي الثلاثي الابعاد مع افتراض وجود ترابط كلي بين المونة و حديد التسليح . جرى الاخذ بنظر الاعتبار اللاخطية للمادة الناتجة عن تشقق وانسحاق المونة والتصرف اللاخطي لعلاقة الاجهاد والانفعال للمونة.تم مقارنة النتائج العملية مع النتائج النظرية وكانت مقبوله.

INTRODUCTION

Ferrocement is a type of thin wall reinforced concrete commonly constructed of hydraulic cement mortar reinforced with closely spaced layered of continuous and relatively small size wire mesh. The mesh may be made of metallic or other suitable materials. Since advanced fiber reinforced polymeric meshes, such as carbon, Kevlar, spectra and the like are available for use in its construction, ferrocement can also be considered a high performance laminated cementitious composite. Most researches reviewed in this paper are found to be the analytical methods predicted the ultimate capacity of members. The nonlinear analysis methods of ferrocement members predicted the ultimate moment capacity in addition to different types of stress. Two main points were noticed from this review: Firstly most of the studies had neglected the tensile stresses of mortar in the analytical methods and secondly they have applied two dimensional element approaches only in the nonlinear analysis.

A general methodology was proposed for the analysis and design of ferrocement flexural elements by Naaman and Homeric [1]; by considering the ferrocement beams as reinforced concrete members subjected to pure bending. The particular aspects of ferrocement such as mesh efficiency and mesh volume content has been integrated in the analysis, thus offering a method within the scope of converge of the ACI Building Code-83. A computerized evaluation was described and a comparison between experimental observation and analytical prediction is given. Mansur[2] presented analytical and experimental investigations of the ultimate load behavior of ferrocement in flexure. The predictions of the three methods A, B and C as outlined above have been compared with the available test data. The rigid-plastic analysis appears to be marginally better. Using this method, design charts have been developed for a typical ferrocement flexural member.

The flexural rigidity and deflection characteristics of ferrocement "flanged" beams (I-and box- beams); number of wire mesh layers in flanges and webs; effect of skeletal steel; and beam length have been considered. Mathematical methods to predict flexural rigidities and deflections of ferrocement" flanged" beams at service load level were also presented by Alsulaimani and Ahmad [3]. The ACI and CEB methods for deflection calculations were used to predict the deflection of ferrocement "flanged" beams. The flexural rigidities in the uncracked and cracked stages for box-beams are larger than those for I-beams for the same steel-reinforcement.

Bin-Omar et al. [4] developed a computational model based on the Timoshenko beam finite element formulations for predicting the entire nonlinear behavior of ferrocement beams of I-type and box type under monotonically increasing loads up to failure using a layered approach. Quadratic isoperimetric elements with three degrees of freedom were used. The ferrocement material adopted in this work was treated as a single material whose properties represent the integrated response of its constituents; mortar and wire mesh. The uniaxial stress- strain relationship has been adopted during the analysis.

Anisotropic elastoplastic models to simulate the mechanical behavior of ferrocement plates were proposed by Arif and Kaushik [5]. These models used elastic and inelastic properties derived from simple in-plane tension and compression experimental tests. Mindlin plate theory in conjunction with a layered approach was employed for analysis. Two different mathematical models, the

homogeneous layered model and the mortar-ferrocement layered model, were considered. The former assumes all the layers to process identical an isotropic material property.

In the present study the analytical procedure is proposed to analyze the flexural members under general case of loading and with different cross sections (rectangular section and T-section). The nonlinear analysis methods of ferrocement members predicted the ultimate moment capacity in addition to different types of stress. The tensile stresses of mortar in the analytical methods are computed. The layering approach for wire mesh reinforcement and embedded approach of skeletal reinforcing bar are used in three dimensional nonlinear analyses. The results of the proposed method and finite element method are compared with experimental work study.

FINITE ELEMENT FORMULATION AND MODELS

The finite element method is a numerical technique for obtaining approximate solutions to a wide variety of engineering problems. Although the method was originally developed to study the stresses in complex airframe structures, it has been extended and applied in continuum mechanics. Because of its flexibility as an analysis tool, it has received much attention in engineering schools and in industry [6]. In the present work, a three dimensional isoparametric finite element model has been used to analyze the ferrocement slabs and beams. The three-dimensional isoparametric element was used to represent the mortar, and the two-dimensional layered approach was used to model the wire meshes in addition to the one-dimensional representation of model skeletal reinforcing bars. The three-dimensional isoparametric quadratic brick element with 20 node and curved boundaries Figure(2.1) was used throughout this study to represent the mortar.

In the brick element, each node has three translational degrees of freedom u, v, and w along the Cartesian coordinates x, y, and z respectively. The Cartesian coordinates (x, y, z) at any point within the isoparametric elements can be obtained by the interpolation shape functions [7, 8, 9]. For three-dimensional finite elements, the strain components are usually be defined in terms of the Cartesian coordinate system (x, y, z). The coordinate system is the most convenient system for expressing the strain and stress components, Therefore the strain vector and (the three normal stresses and three shear stresses) at each Gaussian point are calculated using the constitutive relation given by Ref.[10]

Smeared Representation of Wire Mesh Reinforcement

Smeared representation of steel wire mesh may be used both when the wires are placed in one or two directions. In this formulation, the layer thickness is equivalent to the area of the actual steel per unit length with uniaxial stress characteristics in the direction of the wires. So that in the case of two way steel reinforcement, two different layers are assumed for steel in two directions. Each layer is located at a constant depth from the mid-surface through the thickness of the element, as shown in Figure (2.2).

The Cartesian coordinates (x, y, z) at any point of the wire mesh can be obtained by the interpolation shape functions that are used to define the geometry of the element and the displacement field as Ref.[11]:

Perfect bond is assumed to occur between the mortar and the wire meshes, so that the steel strain-displacement relation is:

$$\begin{Bmatrix} e_x' \\ e_y' \\ g_{xy}' \end{Bmatrix} = \begin{Bmatrix} \frac{\partial u'}{\partial x'} \\ \frac{\partial v'}{\partial y'} \\ \frac{\partial u'}{\partial y'} + \frac{\partial v'}{\partial x'} \end{Bmatrix} \qquad (2.1)$$

In this approach the wire mesh is represented by a number of smeared layers to be distributed over the element with an equivalent thickness in any specified direction in ξ and η plane with an equivalent thickness. The stresses are determined at the Gauss points laying on the mid surface of each layer and these stresses are assumed to be constant over the thickness of the layer, as shown in Fig. (2.3). The layers may have different thicknesses and they can be of different number of layers for different elements. Each wire mesh deforms only in the direction of the mesh and having strength and stiffness characteristics in the mesh direction only. Therefore, it exhibits a uniaxial response. The wire mesh strains and the strains of the surrounding mortar are the same.
The stresses can be determined as

$$\begin{Bmatrix} s_x' \\ s_y' \\ t_{xy}' \end{Bmatrix} = [D_E] \begin{Bmatrix} e_x' \\ e_y' \\ g_{xy}' \end{Bmatrix} \qquad (2.2)$$

where,

$$[D_E] = \begin{bmatrix} E_S & 0 & 0 \\ 0 & 0 & 0 \\ 0 & 0 & 0 \end{bmatrix} \qquad (2.3)$$

The stress s'_K along the layered element is determined from the strain and stress components in the local coordinates of the element in the mesh direction as

$$s'_K = s'_X \cos^2 q + s'_Y \sin^2 q + t'_{XY} \cos q \,.\sin q \qquad (2.4)$$

where q is the angle between the mesh axis and the element local axis x'
The stiffness matrix $[K]_w$ is computed by summing up the contribution of each layer at Gauss points and may be written as:

$$[K]_w = \int_{-1}^{+1}\int_{-1}^{+1} \sum_{i=1}^{NL} [B]_i^T [D]_{wi} [B]_i \, |J| Dz_i \, dx \, dh \qquad (2.5)$$

where NL is the number of layer, $[B]_I$ is the strain matrix calculated at the mid-surface of each layer, $[D]_{wi}$ the material matrix of wire layer,| J | is the determinant of the Jacobian matrix for layer I, and $Dz_i = \frac{2Dhi}{hl}$,(hl is defined the thickness of element).

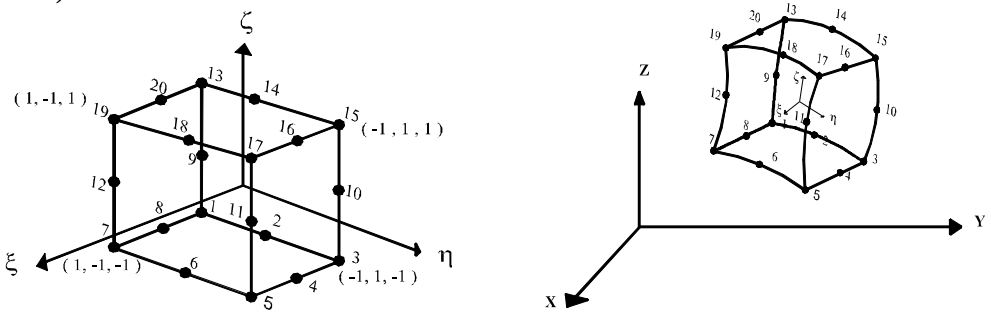

a) Local coordinates. **(b) Cartesian coordinates.**

Figure (2.1): Twenty-node isoparametric brick element used to model the mortar.

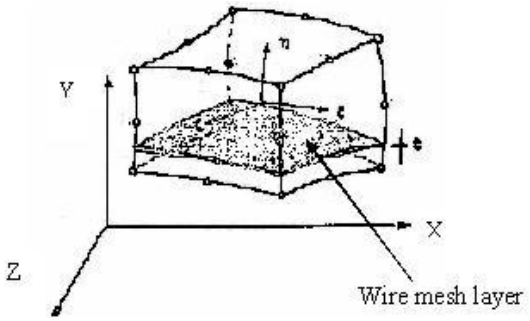

Figure (2.2): Three-dimensional solid element with layered system.

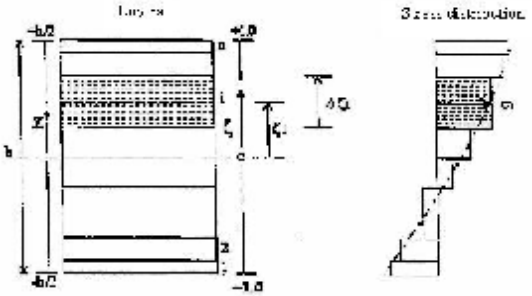

Figure (2.3): Layered model and corresponding stressof wire mesh. representation.

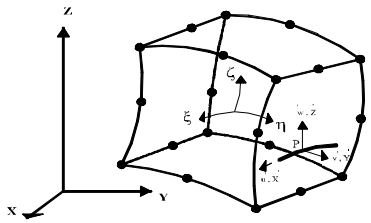

Figure (2.4): Embedded representation of reinforcement.

Embedded Bar Reinforcement Idealization

In the present study, the embedded bar representation of skeletal steel reinforcement bars was represented. The reinforcing bar is considered to be an axial member built into the is oparametric mortar element, Figure (2.4). The assumption of compatibility of displacements and strains between the steel and

mortar allows the reinforcing bars to be treated as integral part of the element. In this approach perfect bond is assumed to occur between the reinforcing bars and

The surrounding mortar. The reinforcing bars are assumed to be capable of transmitting axial forces only [11, 12].

Numerical Integration

The numerical integration is required to set up the stiffness matrices and the equivalent nodal loads. For the elements adopted in this study, the Gauss quadrature method has been used. The integration points are also the sampling points for stresses and material state determination.

The integration rules which have been used in this study for two and three-dimensional elements are,

- The 2 or 3 Gauss-integration rule for embedded bar.
- The 9 (3x3) Gauss-quadrature for smeared layered wire mesh.
- The 27 (3x3x3) Gauss-quadrature integration rules for brick element.

The distribution of sampling points in the 9 point rule and 27 point rule of integration and the weights and locations of the gauss points are given in Refs.[10].

Modeling Of Material Properties

Ferrocement is a composite material consisting of mortar and steel (mesh and skeletal) reinforcement. These materials have widely different properties. The present section describes the theoretical developments and the numerical models used for the analysis of ferrocement members.

Models Used For Mortar

The material model used in this study is suitable for the nonlinear static analysis of three dimensional ferrocement members under monotonically increasing load. The material models for mortar in compression and in tension that are used in this study are given in the following sections.

Modeling Mortar In Compression

The behavior of mortar in compression is simulated by an elasto-plastic work hardening model followed by a perfectly plastic model, which is terminated at the onset of crushing. The plasticity model will be illustrated in terms of the following constituents [10].

a- The Yield Criterion

The yield criterion determines the stress level at which the plastic deformation begins. For an isotropic material, the initial yield criterion should be independent of the orientation of the coordinate system in which the stress state is defined and therefore it should be a function of the three stress invariants only [10]. However, a yield criterion dependent on two stress invariants has proved to be adequate for most practical situations and it can be expressed as:

$$f(\{s\}) = c\, I_1 + \left[(c\, I_1)^2 + 3\, b\, J_2\right]^{\frac{1}{2}} = s_o \qquad (2.6)$$

where:

$$I_1 = s_x + s_y + s_z \qquad (2.7)$$

$$J_2 = \frac{1}{3}\left[\left(s_x^2 + s_y^2 + s_z^2\right) - \left(s_x s_y + s_y s_z + s_z s_x\right)\right] + t_{xy}^2 + t_{yz}^2 + t_{zx}^2 \qquad (2.8)$$

Where c, β are material parameters, I_1 is the first stress invariant ,J_2 is the second deviatoric stress invariant and S_o is the equivalent effective stress taken from uniaxial tests. The parameters c and β, can be determined from the uniaxial compression test and the biaxial experimental results under equal compression stress [13]. A relation between the biaxial compressive yield stress (f_{cb}) and the uniaxial compressive yield stress (f_c') can be used as (f_{cb} =1.16 f_c') then the value of the constant c and β are.

$$c = 0.17734 \qquad (2.9)$$
$$b = 1.35468$$

According to the experimental results obtained in the present research work, the initial yield surface in the strain hardening model is attained when the effective stress s_o reaches (25%) of the ultimate stress (f_c').

$$s_o = C_p f_c' \qquad (2.10)$$

Where C_p is the plasticity coefficient which is equal to 0.25 for mortar.

b- Hardening Rule

The hardening rule defines the expansion of subsequent yield surfaces during plastic loading. A number of hardening rules have been proposed to describe the growth of subsequent loading surfaces for a work hardening material [10]. Since only a monotonic loading is considered, the assumption of isotropic hardening model has been adopted in the present work. The initial yield surface is assumed to expand uniformly without distortion as plastic deformation occurs.

The effective stress and the effective plastic strain are used to allow for extrapolation from the results of a uniaxial test to the multiaxial states. The equivalent stress-strain relation beyond the limit of elasticity can be obtained from the uniaxial compressive stress-strain curve. In the present study a parabolic stress-strain relationship has been used in which a zero magnitude is assumed for plastic strain component at the initial yield point equal to $C_p f_c'$. At the peak compressive stress f_c', the total strain has a value e_o, The stress-strain relationship adopted in the present work is expressed as follows [10].

c- Flow Rule

To construct the stress-strain relationship in the plastic range, an associated flow rule will be employed. This means that the plastic deformation rate vector will be assumed to be normal to the current loading surface. The plastic strain increment is then defined as [10].

d- Crushing Condition

The crushing type of mortar fracture is a strain controlled phenomenon. A failure surface in the strain space must be defined in order to take this type of failure into account. Lack of available experimental data has resulted in the failure surface being developed by simply converting the yield criterion described in terms of stresses directly into strains [10].

TENSION BEHAVIOR AND CRACKING MODEL

a - Cracking Model

In the finite element analysis two mainly approaches have been employed for crack modelling. These approaches are discrete cracking model and smeared cracking model. The discrete cracking model can appear only at the element boundaries [10]. In the smeared cracking model, the mortar is assumed to remain a continuum that is the, cracks are "smeared-out" in a continuous fashion. For most structural engineering applications the smeared cracking model is used.

Modeling of Reinforcement

The mechanical properties of reinforcement (wire meshes and skeletal bars) are well-known in comparison to mortar. The reinforcing bars and wire meshes are homogeneous and have usually the same yield strength in tension and compression. A bilinear uniaxial stress-strain relationship allowing for strain hardening and elastic unloading is used [10].

Analytical Modelling

The purpose of this analytical study is to develop a model that accurately predicts the flexural behavior of ferrocement cross sections. The model can also be used to predict the nominal moment and ultimate load. The finite difference technique is used to obtain the deflection at each section of the member.

The model employs strain compatibility, force and moment equilibrium and the following assumption.

1- Plane section remains plane after bending.
2- Small flexural deformations and linear strain distribution through the cross section.
3- Perfect bond between mortar and wire mesh reinforcement or skeletal reinforcement bar is assumed to occur.
4- Axial deformation, shear deformation and torsional effects are neglected.

The model was based on the internal forces, internal moments, strains, and stresses in the cross section as shown in Fig. (3.1).The forces in the compression mortar section and in the tension mortar section will be calculated by direct integration. For each level of strain the cross section divided into several layers and determines the strain in each layer from a linear distribution of strains and an assumed position for the neutral axis. The stress in each layer is then obtained from the calculated strains and stress-strain relationships specified for the mortar and wire mesh reinforcement and skeletal bar reinforcement. The assumed position of the neutral axis is then adjusted until section equilibrium is reached and the internal moment is calculated. The moment of inertia of cross section is calculated to obtain the deflection in each section. The process is repeated for several levels of compression strain including first cracking, maximum moment strength, and

ultimate strength until the compressive strain of mortar exceed the ultimate compressive strain of mortar.

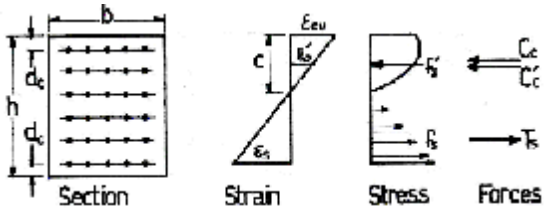

Figure (3.1): Strain force distribution in ferrocement section at ultimate.

Constitutive Relationships for Materials under Stress

Compression and Tensile Stress-Strain Relationship of Mortar

In the present work the plain concrete stress-strain behavior in compression is described for mathematical mortar stress –strain curve. Namman [1] proposed the significance of the experimental stress-strain curve for mortar with the mathematical curve for plain concrete. The Hognestand's stress-strain relation of concrete in compression is employed in this study, which is one of the most generally used equations to model the constitutive behavior of concrete. Fig.(3.2) exhibits the typical stress-strain relation of concrete in compression [14].

The Hognestad parabola describing the ascending branch of the stress-strain curve shown in Fig.(3.2) can be expressed as follows:

$$f_c = f_c' \left[\frac{2e_c}{e_o} - \left(\frac{e_c}{e_o} \right)^2 \right] \quad if \quad 0 \le e_c < e_o \tag{3.1}$$

The descending branch as follows:

$$f_c = f_c' \left[1 - \frac{0.15}{e_u - e_o} \left(e_c - e_o \right) \right] \quad if \quad e_o \le e_c \le e_u \tag{3.2}$$

$$e_o = \frac{2 f_c'}{E_c} \tag{3.3}$$

Where,

f_c' = the maximum cylinder compressive stress of concrete.

e_c = concrete strain at any given point.

e_o = the strain at the maximum compressive stress of concrete.

e_u = ultimate concrete strain.

E_c = the modulus of elasticity of concrete.

The average (or smeared) Stress- strain curve of concrete in tension [15] is shown on Fig. (3.3) where ascending and descending branches are given as:

$$f_t = E_c\, e_t \qquad e_t \le e_{cr} \qquad (3.4)$$

$$f_t = f_{cr}\left(\frac{e_{cr}}{e_t}\right)^{0.4} \qquad e_t > e_{cr} \qquad (3.5)$$

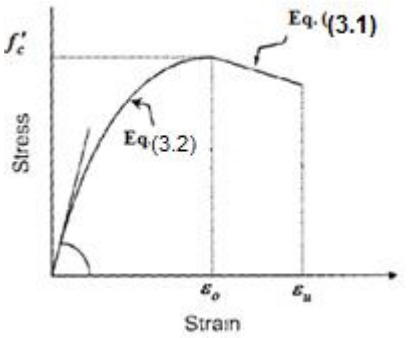

Figure (3.2): Stress-strain relationship of concrete in compression [14].

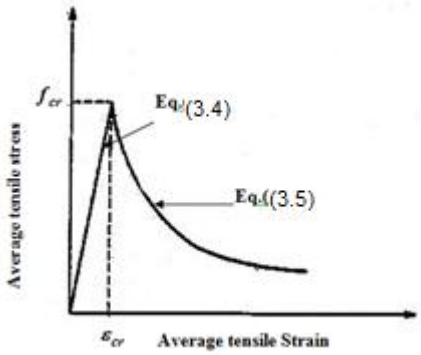

Figure (3.3): Average tensile stress-strain curve for concrete [15].

Tensile Stress-Strain Relationship of Steel Reinforcement

A typical bilinear elastic-perfectly plastic behavior is assumed for wire mesh reinforcement and skeletal bar reinforcement, as shown in Fig. (3.4). However, in the present study, which aims to analyze cracking in the serviceability state, it is appropriate to consider the initial elastic slope only, and not the plastic branch. Therefore, to describe the actual behavior of the steel a typical linear relationship can be considered:

$$f_s = E_s\, e_s \qquad e_s \le e_y \qquad (3.6)$$

$$f_s = f_y \qquad e_s > e_y \qquad (3.7)$$

Where, f_s, e_s tensile stress and strain of reinforcement respectively, e_y yield strain of reinforcement, and f_y yield stress of the reinforcement.

Internal Forces and Moments Contributed by Mortar

The force and moment in the mortar section will be calculated by direct integration. In order to perform the integration, the compression and tension zone of the cross section has been divided into several layers (parts) [16].

Strain Distribution of Wire Mesh and Skeletal Bar Reinforcement

To calculate the forces in each layer of wire mesh the steel area for each layer will be needed. There are two assumptions to obtain the area of each layer. The first will be depended on the repeating section for each type of mesh. This assumption is used in this study. The second will be depended on the volume of friction [17]:

By using strain compatibility, the corresponding strains for the tensile reinforcing of wire meshes, compressive reinforcing of wire meshes, tensile reinforcing of skeletal bars and compressive reinforcing of skeletal bars are calculated by Ref. [16]. The tensile and compressive (forces and moments) for wire meshes and skeletal bars in tension and compression zone are calculated by Ref [16].

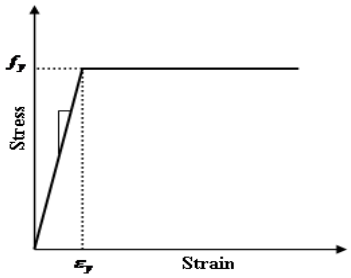

Figure (3.4): Stress-strains of wire mesh and skeletal bar reinforcement.

Calculation of Sectional Deflection

In order to calculate the deflection at a certain stage of loading and at any position of section, the fourth order differential equation given by:

$$\frac{d^4W}{dx^4} = \frac{q}{E_c I} \qquad (3.8)$$

$$\frac{d^2W}{dx^2} = \frac{-M}{E_{cm} I} \qquad (3.9)$$

$$I = I_{mc} + I_{mt} + I_{steel}$$

These equations have been solved using the finite difference method where:

W: vertical deflection

M: the bending moment.

q: applied load.

I : average moment of inertia about the neutral axis of the cross section at any segment of the beam length, and at any level of loading where the deflection is to be calculated.

E_{cm} : modulus elasticity of the mortar.

I_{mc} : the moment of inertia of compression mortar zone.

I_{mt} : the moment of inertia of tension mortar zone.

I_{steel} : the moment of inertia of wire meshes and skeletal bars reinforcement.

Numerical Applications

This section presents the numerical applications on ferrocement members using the suggested analytical and finite element models. The finite element

analyses are carried out to investigate the behavior of ferrocement flexural members by using the algorithm procedure presented in section 2 through the use of (3DLFERRO) computer program developed in the present research work. The results obtained using both the analytical and finite element models are compared with the experimental results through the load-deflection curves. An investigation has also been carried out to study the distribution of normal strains and normal stresses along the depth of midspan cross section of the flexural members. Also moment-curvature plots obtained using the analytical and numerical models were compared with the experimental results carried out in this study work.

Analysis of Rectangular Beams of Group A

For the simply supported rectangular beam specimens of group A. details of wire mesh reinforcement and geometry for each beam are based on (Table.4.1). Material properties adopted for the proposed analytical and finite element models are listed in Table (4.2).

Results of Analysis of Rectangular Beams of Group A

a)Load Deflection Curves

For all rectangular beams of group C which were analyzed using the proposed analytical and finite element methods, the experimental and predicted load-midspan deflection curves are shown in Figs. (4.1) to (4.4). For all analyzed beams the finite element solutions are generally in good agreement with the experimental results throughout the entire range of loading. The arrangement of reinforcement within the cross section indicates slightly softer results for the proposed analytical method as compared with the experimental data. The comparison between the analytical and finite element predicted ultimate loads with the experimental ultimate loads is shown in Table (4.3).

b)Moment Curvature Response

This study has been conducted to find out the moment-curvature response throughout the entire loading history by applying the proposed analytical and finite element methods. The results are shown in Figs. (4.5) to (4.8) for rectangular beams of group A.

All the specimens have almost the same predicted linear moment curvature relations before cracking. After cracking the curvature increases at an increasing rate as the applied loads are increased up to failure. The analytical response shown in the figures at early stages is similar to the finite element response. For stages after cracking and stages close to the ultimate load the analytical moment curvature response is softer than the corresponding finite element response.

Table (4.1) Details of testing specimens.

Group	Type of members	Specimen designation	Diameter of wire mesh (mm)	No. of wire mesh layers
A	Rectangular beam section ,L=1200mm	R1	0.6	2
		R2	0.8	2
		R3	0.8	3
		R4	0.8	3+Skeletal bars

Table (4.2) Material properties used for rectangular beams of group A.

		R1	R2	R3	R4
Mortar					
E_c	Young's modulus (MPa)	22647	22647	22647	22647
$f_c^{\cent}$	Compressive strength (MPa)	30.0	29.0	27.8	28.5
f_r	Modulus of rupture (MPa)	3.65	3.65	3.65	3.65
n^*	Poisson's ratio	0.2	0.2	0.2	0.2
Wire mesh reinforcement					
E_S	Young's modulus (MPa)	175000	85000	85000	85000
f_y	Yield stress (MPa)	350	170	170	170
Skeletal bar reinforcement					
E_S	Young's modulus (MPa)	--	--	--	200000
f_y	Yield stress (MPa)	--	--	--	400

* Assumed value

Table (4.3) Comparison of ultimate load P_u (kN) for rectangular beams of group A.

Specimens	Exp. P_u	Analytical model		FEM	
		P_u	$\frac{P_u}{P_{u\,exp}}$	P_u	$\frac{P_u}{P_{u\,exp}}$
R1	4.75	4.32	0.909	4.8	1.011
R2	4.125	3.68	0.892	4.08	0.989
R3	6.375	5.82	0.913	6.35	0.996
R4	10.5	9.48	0.903	9.7	0.924

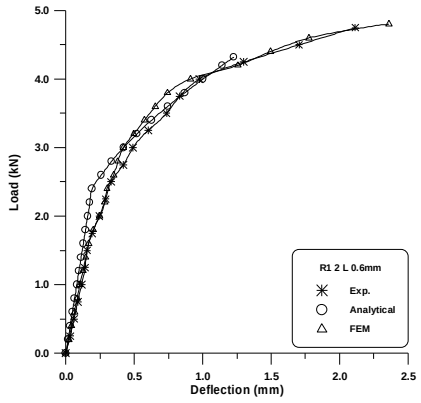

Figure (4.1): Experimental and predicted load-midspan deflection curves of rectangular beam R1

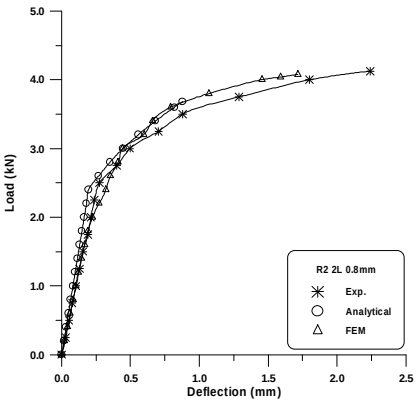

Figure (4.2): Experimental and predicted load- midspan deflection curves of rectangular beam R2

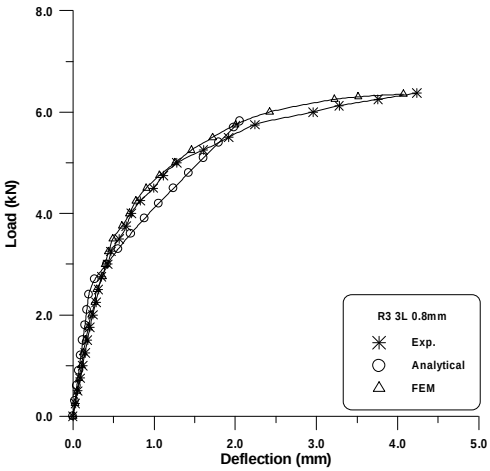

Figure (4.3): Experimental and predicted load-midspan deflection curves of rectangular beam R3

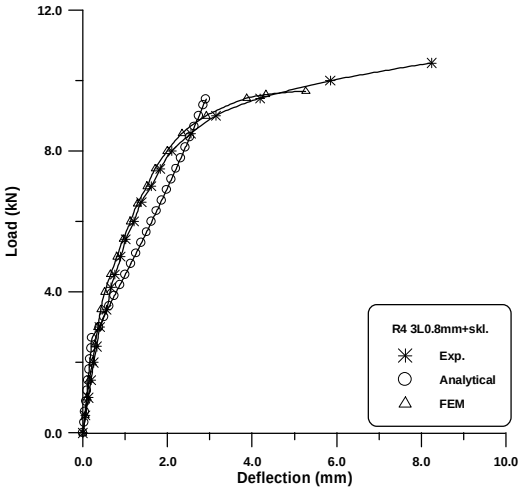

Figure (4.4): Experimental and predicted load-midspan deflection curves of rectangular beam R4

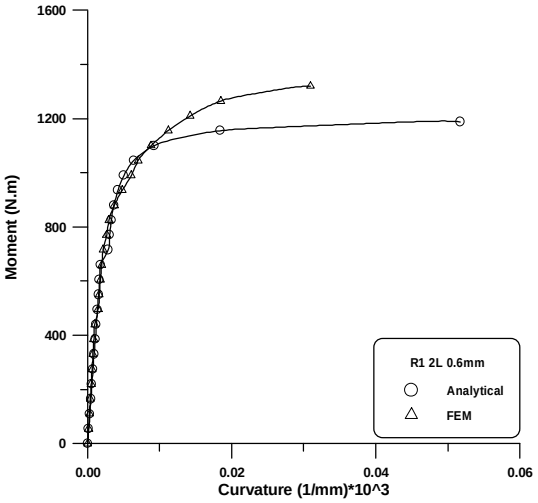

Figure(4.5): Numerical and analytical moment-midspan curvature response of rectangular beam R1

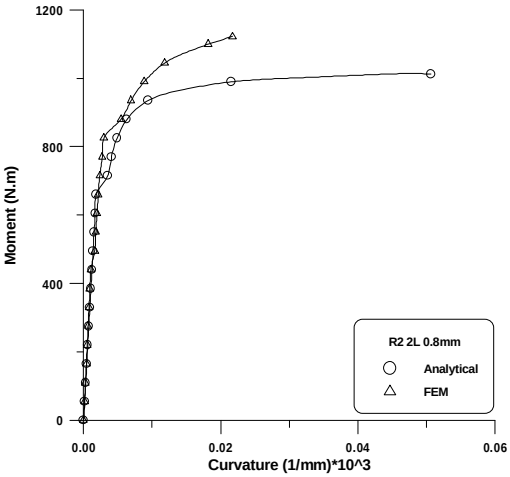

Figure (4.6): Numerical and analytical moment-midspan curvature response of rectangular beam R2

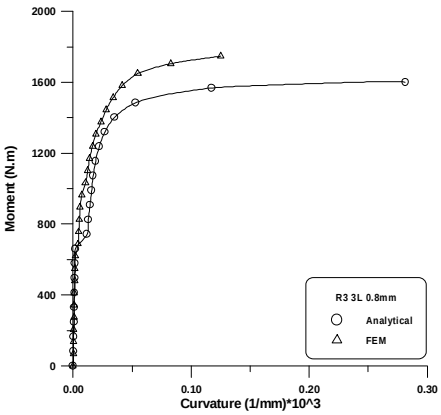

Figure(4.7): Numerical and analytical moment-midspan curvature response of rectangular beam R3

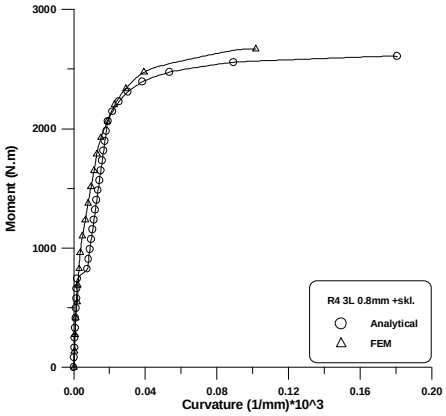

Figure (4.8): Numerical and analytical moment-midspan curvature response of rectangular beam R4

FINITE ELEMENT ANALYSIS OF T-BEAMS OF GROUP B

Finite Element Idealization and Material Properties

For the simply supported T-beam specimens of group B. details of wire mesh reinforcement and geometry for each beam are based on (Table.4.4). Material properties adopted for the proposed analytical and finite element models are listed in Table (4.5).

Results of Analysis of T-beams of Group B

a) Load Deflection Curves

Figure (4.9) indicates that both the proposed analytical and the finite elements results for T-beam specimen T1 depart from the experimental results. The finite element solution indicates that the wire meshes located at bottom face of the beam had yielded and then crushing of mortar took place at the ultimate load. At ultimate stages the analytical response is slightly stiffer than the experimental curves. On the other hand good agreement for both analytical and numerical methods has been noticed as compared with the experimental results of beams T2 and T3 as shown in Figures. (4.10) and (4.11). The comparison between the analytical and finite element predicted ultimate loads with the experimental ultimate loads is shown in Table (4.6)

b) Moment Curvature Response

By applying the proposed analytical and finite element methods the moment curvature curves are shown in Figures. (4.12) to (4.14) for T-beams of group B. This study has been conducted to find out the moment-curvature response throughout the loading stages.

The specimens have almost the same behavior linear moment curvature relations before cracking. After cracking, the curvature increases at an increasing rate as the applied loads are increased up to failure. The finite element results showed a response softer than the proposed analytical results for beam T1. While, the analytical responses for beams T2 and T3 shown in Figures. (4.13) and (4.14) respectively, are softer than the corresponding finite element responses at early stages after cracking stages and stages close to ultimate load.

Table 4.4 Details of testing specimens.

Group	Type of members	Specimen designation	Diameter of wire mesh (mm)	No.of wire mesh layers
B	T-section beam , L=1200 mm	T1	0.8	2
		T2	0.8	3+Skeletal bars
		T3	0.6	3+Skeletal bars

Table (4.5) Material properties used for T-beams of group B.

		T1	T2	T3
Mortar				
E_c	Young's modulus (MPa)	22647	22647	22647
$f_c^{\cent}$	Compressive strength (MPa)	29.0	28.5	28.8
f_r	Modulus of rupture (MPa)	3.65	3.65	3.65
u*	Poisson's ratio	0.2	0.2	0.2
Wire mesh reinforcement				
E_S	Young's modulus (MPa)	85000	85000	175000
f_y	Yield stress (MPa)	170	170	350
Skeletal bar reinforcement				
E_S	Young's modulus (MPa)	--	200000	200000
f_y	Yield stress (MPa)	--	400	400

*Assumed value

Table (4.6) Comparison of ultimate load P_u (kN) for T-beams of group B.

Specimens	Exp. P_u	Analytical model		FEM	
		P_u	$\frac{P_u}{P_{u\,exp}}$	P_u	$\frac{P_u}{P_{u\,exp}}$
T1	4.15	3.96	0.954	4.04	0.973
T2	12.0	11.48	0.956	11.8	0.983
T3	14.0	12.79	0.914	13.2	0.943

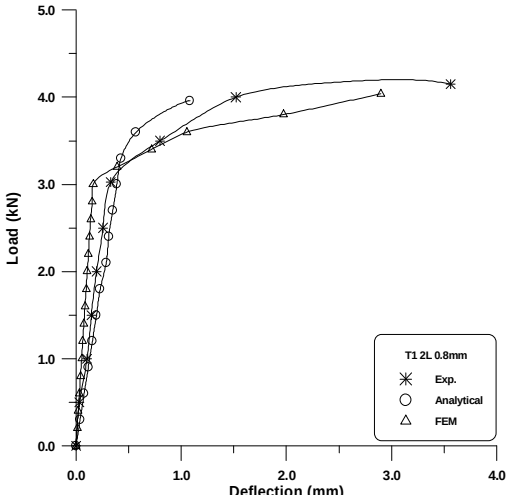

Figure (4.9): Experimental and predicted predicted load-midspan deflection curves of T-beam T1

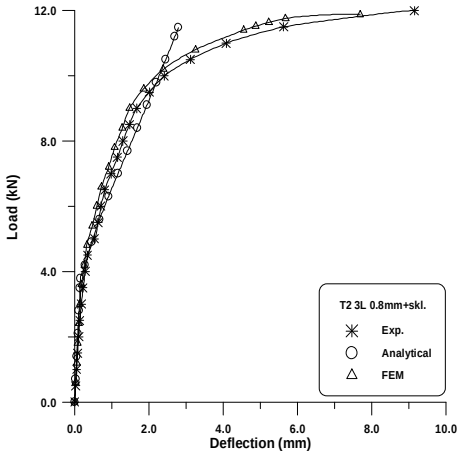

Figure (4.10): Experimental and load-midspan deflection curves of T-beam T2

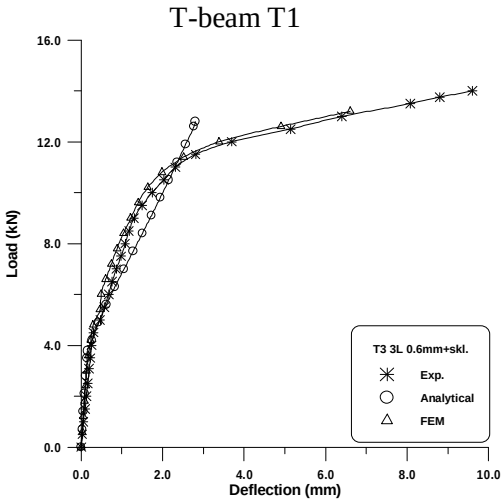

Figure (4.11): Experimental and predicted load-midspan deflection curves of T-beam T3

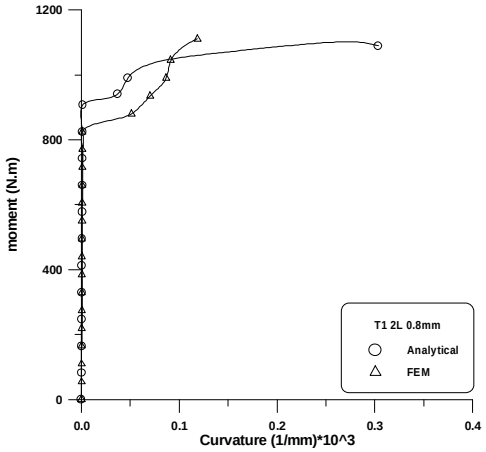

Figure (4.12): Numerical and analytical moment-midspan curvature curves of reeponse T-beam T1

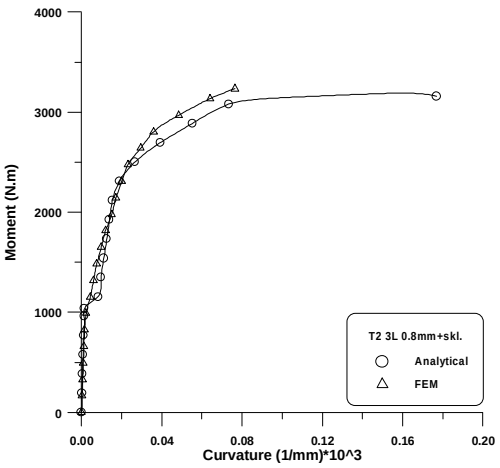

Figure (4.12): Numerical and analytical moment-midspan curvature curves of T-beam T2

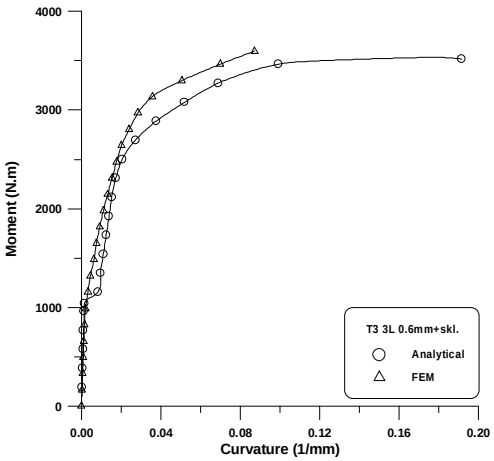

Figure (4.12): Numerical and analytical moment-midspan curvature curves of T-beam T3

CONCLUSIONS

By comparing of proposed analytical and numerical results with corresponding experimental data, the following conclusions are drawn.

1. It is found that the predicted response obtained using the proposed analytical and finite element models are close to experimental response at early stages before cracking. The post cracking response and the behavior close to the ultimate load obtained using the proposed analytical methods is relatively softer than the experimental behavior, while the predicted finite element response all stages after cracking is close to the experimental behavior.
2. The moment-curvature response throughout the entire loading history of one way slabs, rectangular beams and T-beams is predicted by applying the proposed analytical and finite element models. At early stages of loading, the analytical response and the finite element response are almost similar. For stages after cracking and stages close to the ultimate load, the analytical moment curvature response is relatively softer than the corresponding finite element behavior this can be attributed ignoring the effect of residual post cracking tensile stress of mortar in the analytical model.
3. The load carrying capacity of the tested ferrocement members is closely predicted using both the proposed analytical method and the finite element analysis. For the rectangular beam specimens, the ratio ranged loads to the experimental ultimate loads between 0.892 and 0.913 for the proposed analytical method and ranged between 0.924 and 1.011 for the finite element analysis. While for the T-beam specimens, the ratio of ultimate loads ranged between 0.914 and 0.956 for the proposed analytical method and ranged between 0.943 and 0.983 for the finite element analysis.

REFERENCES

[1].Naaman, A.E. Homeric, J.R., "Flexural Design of Ferrocement Computerized Evaluation and Design Aids", Journal of Ferrocement Vol.16, No.2, April 1986, pp 101-116.

[2].Mansur, M.A., "Ultimate Strength Design of Ferrocement in Flexure", Journal of Ferrocement, Vol.18, No.4, October- 1988, pp.385-395.

[3].Alsulaimani, G. J. and Ahmad, S. F., "Deflection and Flexural Rigidity of Ferrocement I- and Box-Beams", Journal of Ferrocement, Vol.18, No.1-January, 1988, pp. 1-11.

[4].Bin-Omar, A.R., Abdel-Rahman, H. H. and Al-Sulaimani, G. J., "Nonlinear Finite Element Analysis of Flanged Ferrocement Beams", Computers & Structures, Vol.31, No.4,1989, pp. 5810-590.

[5].Arif, P.M. and Kaushik, S., "Mechanical Behavior of Ferrocement Composites Numerical Simulation", ASCE, Journal of Materials in Civil Engineering, March-April 2002, pp. 156-163.

[6].Huebner, K.H., and Thornton, E. A., "The Finite Element Method for Engineers", 2nd Ed., John Wiley and Sons, New York, 1982, 623 p.

[7].Zienkiewicz, O. C., "The Finite Element Method in Engineering Science", McGraw-Hill, London, 1971, 521 p.

[8].Cook, R.D., "Concepts and Applications of Finite Element Analysis", 2nd Ed., John Wiley and Sons, New York, 1981.

[9].Taylor, R.L., "On Completeness of Shape Functions for Finite Element Analysis", IJNME, Vol. 4, No.1, 1972, pp.17-22.

[10].Al-Shaarbaf, I.A.S., "Three-Dimensional Nonlinear Finite Element Analysis of Reinforced Concrete Beams in Torsion", Ph. D. Thesis, University of Bradford, 1990, 323 p.

[11].Phillips, D. V., and Zienkiewicz, O. C., "Finite Element Nonlinear Analysis of Concrete Structures", Proc. Inst. Of Civil. Engineering, Vol. 61, Part 2, March 1976, pp. 59-88.

[12].Kopal, Z., "Numerical Analysis", John Wiley and Sons, New York, 1955.

[13].Kupfer, H., Hilsdorf, H. K., and Rusch, H., "Behavior of Concrete under Biaxial Stresses", ACI Journal, Vol.66, No. 8, August 1969, pp.656-666.

[14].Park, R. and Paulay, T. "Reinforced Concrete Structures", John Wiley and sons, New York, 1975.

[15].-Hsu, T.T.C., "Unified Theory of Reinforced Concrete", CRC Inc., 1993, 313p.

[16].Mohammed N.S., “Analysis and Ultimate Capacity of Ferrocement Flexural Members”, Ph. D. Thesis, University of Technology,2007 ,206 p.

[17].Noury, S.I.A. and Huq, S., "Ferrocement in Axial Tension", Journal of Ferrocement Vol. 18. No.2, April-1988, pp.111-137.